Calculating Static Field and Charge Distributions Using a Full-Wave Boundary Element Method

Haixin Ke and Todd Hubing, *Fellow, IEEE*

Department of Electrical and Computer Engineering, Clemson University, Clemson, SC 29634 USA

In order to model configurations driven by broadband sources (e.g., digital signals), it is desirable to employ a full-wave modeling technique that works well at both high and low frequencies. This paper describes a method for improving the low-frequency performance of existing full-wave boundary element techniques and demonstrates how the full-wave model can be used to solve static electric field problems. The new approach performs linear transformations on the moment matrix utilizing an LU decomposition and matrix reconstruction. It does not require special basis functions and is relatively easy to implement in existing boundary element codes. Examples presented demonstrate how modified full-wave software is capable of calculating static field and charge distributions for a variety of configurations using the same algorithms and the same input used to do high-frequency calculations.

***Index Terms*—Charge distribution, full-wave method.**

I. Introduction

MOST full-wave numerical electromagnetic modeling techniques lose accuracy and become unstable at very low frequencies. These instabilities can be explained in terms of the natural Helmholtz decomposition of Maxwell's equations or attributed to the imbalance between the vector and scalar potentials. Various methods have been developed to overcome these instabilities, such as using loop-tree or loop-star formulations [1]–[4] or switching to static or quasi-static methods.

Loop-tree or loop-star formulations generally involve the construction of special basis functions that depend on the geometry and the mesh of the model. An imbalance between vector and scalar potential terms remains even if the numerical error is reduced. These formulations generally require software that is tailored to specific types of geometries and are not well suited to general purpose modeling codes.

Many static or quasi-static methods, such as those used to calculate the capacitance of conductors, solve Laplace's equation subject to appropriate boundary conditions [5]–[7]. These methods are based on integral equations, in which the electric potential and charge distribution are related by free space Green's functions. The electric charge densities are determined by forcing the potential function to satisfy the prescribed boundary conditions. Static and quasi-static methods are generally incompatible with high-frequency analysis, since they do not adequately model the interaction between time-varying electric and magnetic fields.

Recently, a technique was introduced for extending the frequency range of full-wave boundary element codes by performing linear matrix transformations on the vector and scalar components of the impedance matrix [8], [9]. This technique allows accurate field calculations to be made at frequencies where the geometries being analyzed are many orders of magnitude smaller than a wavelength. This paper more fully explains this technique and extends it to allow static electric field problems to be solved using this approach.

II. Full-Wave Model Formulation

For a closed perfect electric conductor (PEC) surface S, the electric field integral equation (EFIE) is usually written as [10]

$$\mathbf{E}^{\text{inc}}(\mathbf{r}) = \int_S \begin{bmatrix} jk\eta \mathbf{J}(\mathbf{r}')\mathbf{G}_0(\mathbf{r},\mathbf{r}') \\ -j\frac{\eta}{k}\nabla' \bullet \mathbf{J}(\mathbf{r}')\nabla'\mathbf{G}_0(\mathbf{r},\mathbf{r}') \end{bmatrix} dS' \quad (1)$$

where k is the wave number and η is the intrinsic impedance. $\mathbf{J}$ is the equivalent surface current density, and

$$\mathbf{G}_0(\boldsymbol{r},\boldsymbol{r}') = \frac{e^{-jk|r-r'|}}{4\pi|\boldsymbol{r}-\boldsymbol{r}'|} \quad (2)$$

is the free space Green's function. The integral in (1) is a principal-value integral in which the singularity at $\boldsymbol{r} = \boldsymbol{r}'$ is excluded. The well-known Rao–Wilton–Glisson (RWG) basis functions [11] are often used to expand the surface current density as

$$\boldsymbol{J} = \sum_n J_n \boldsymbol{f}_n. \quad (2a)$$

By applying the method of moments, (1) is formulated into a matrix equation as

$$\mathbf{C} \bullet \mathbf{J} = \mathbf{F} \quad (3a)$$

where $\mathbf{J} = [J_n]$ is a vector of the unknown surface current densities, $\mathbf{F} = [F_m]$ is an excitation vector, and $\mathbf{C} = [C_{\text{mn}}]$ is an $N \times N$ impedance matrix. $\mathbf{C}$ is composed of two parts, $\mathbf{C}_1$ and $\mathbf{C}_2$, corresponding to the left and right terms inside the brackets in (1)

$$[\mathbf{C}_1 + \mathbf{C}_2] \bullet \mathbf{J} = \mathbf{F}. \quad (3b)$$

Digital Object Identifier 10.1109/TMAG.2007.892310

Comparing (3b) to the mixed-potential form of the scattered electric field

$$\mathbf{E}^{\text{sca}} = -j\omega\mathbf{A} - \nabla\Phi \tag{4}$$

it is apparent that $\mathbf{C}_1$ corresponds to the magnetic scalar potential term $-j\omega\mathbf{A}$ and $\mathbf{C}_2$ corresponds to the electric scalar potential term $-\nabla\Phi$.

Solving (3) yields the current density $\mathbf{J}$. The charge density ρ_s is related to the current density by [12]

$$\rho_s = \frac{\nabla \cdot \boldsymbol{J}}{-j\omega} \tag{5}$$

where ρ_s must be finite, suggesting that $\nabla \cdot J$ must be proportional to ω as the frequency goes to zero. ρ_s can be expanded in terms of the basis functions as

$$\rho_s = \frac{-1}{j\omega}\left(\nabla \cdot \sum_n J_n \boldsymbol{f}_n\right) = \frac{-1}{j\omega}\sum_n J_n(\nabla \cdot f_n). \tag{6}$$

III. LU Recombination Method

Full-wave models based on this formulation experience instability at low frequencies when using standard basis functions. This can be seen from the mixed potential expression of the field (4). The vector and scalar potentials do not scale with frequency in the same way. At low frequencies, the magnetic vector potential contributions to the elements of the impedance matrix are insignificant compared to the electric scalar potential contributions. The dominant part, i.e., the scalar potential contribution, depends only on the surface divergence of $\boldsymbol{J}$ [12]. Knowledge of $\nabla \cdot \boldsymbol{J}$ is not sufficient to determine $\boldsymbol{J}$, because the integral over closed loops is zero [13]. This leads to the failure of the E-field solution at low frequencies. Mathematically, $\mathbf{C}_1$ is much smaller than $\mathbf{C}_2$ at low frequencies, and $\mathbf{C}_2$ is singular when there are closed loops in the mesh [8]. So the impedance matrix at low frequencies is nearly singular, and the solution is sensitive to small numerical errors resulting from the cancellation of large numbers when integrating the scalar potential over closed loops.

An LU recombination method was developed to overcome this difficulty [9]. The LU recombination method applies the following decomposition to the impedance matrix $\mathbf{C}$:

$$\begin{aligned}\mathbf{C} &= \mathbf{C}_1 + \mathbf{C}_2 = \mathbf{L}\mathbf{D}\mathbf{L}' + \mathbf{L}\mathbf{U}\mathbf{L}' \\ &= \begin{bmatrix}\mathbf{L}_{ii} & \mathbf{0}\\ \mathbf{L}_{di} & \mathbf{L}_{dd}\end{bmatrix}\left(\begin{bmatrix}\mathbf{D}_{1ii} & \mathbf{D}_{1id}\\ \mathbf{D}_{1di} & \mathbf{D}_{1dd}\end{bmatrix}\right. \\ &\quad \left. + \begin{bmatrix}\mathbf{D}_{2ii} & \mathbf{D}_{2id}\\ \mathbf{D}_{2di} & \mathbf{D}_{2dd}\end{bmatrix}\right)\begin{bmatrix}\mathbf{L}'_{ii} & \mathbf{L}'_{di}\\ \mathbf{0} & \mathbf{L}'_{dd}\end{bmatrix}.\end{aligned} \tag{7}$$

In (7), $\mathbf{L}$ is a lower triangular matrix resulting from the LU decomposition of $\mathbf{C}_2$. $\mathbf{D}_1$ and $\mathbf{D}_2$ are matrices such that $\mathbf{C}_1 = \mathbf{L}\mathbf{D}_1\mathbf{L}'$ and $\mathbf{C}_2 = \mathbf{L}\mathbf{D}_2\mathbf{L}'$. The prime indicates the transpose of the matrix. $\mathbf{C}_2$ is not a full rank matrix. Linearly independent rows in $\mathbf{C}_2$ are grouped together, while dependent rows are moved to the end of the matrix. The same rearrangement is applied to the whole $\mathbf{C}$ matrix so that $\mathbf{L}, \mathbf{D}_1$, and $\mathbf{D}_2$ can be partitioned as in (7), where the subscript i means independent and d means dependent.

The LU recombination method modifies $\mathbf{L}_{di}$ according the linear relationship between rows of $\mathbf{C}_2$. At the same time, it sets $\mathbf{D}_{2dd}$, $\mathbf{D}_{2di}$, and $\mathbf{D}_{2id}$ to zero. The matrix equation to be solved by the LU recombination method is then

$$\begin{bmatrix}\mathbf{D}_{1ii}+\mathbf{D}_{2ii} & \mathbf{D}_{1id}\\ \mathbf{D}_{1di} & \mathbf{D}_{1dd}\end{bmatrix}\begin{bmatrix}\mathbf{J}_i^r\\ \mathbf{J}_d^r\end{bmatrix} = \begin{bmatrix}\mathbf{F}_i^r\\ \mathbf{F}_d^r\end{bmatrix} \tag{8}$$

where

$$\begin{bmatrix}\mathbf{J}_i^r\\ \mathbf{J}_d^r\end{bmatrix} = (\mathbf{L}')^r \cdot \mathbf{J}, \tag{9}$$

and

$$\begin{bmatrix}\mathbf{F}_i^r\\ \mathbf{F}_d^r\end{bmatrix} = (\mathbf{L}^r)^{-1} \cdot \mathbf{F} \tag{10}$$

where the superscript r means modified. Previous work [9] showed that the LU recombination method is capable of solving for the low-frequency currents in simple circuit configurations with good accuracy.

IV. Full-Wave Model at Zero Frequency

As the frequency $\omega \to 0$, the EFIE (1) reduces to

$$\mathbf{E}^{\text{inc}}(r) = \int_S \left[-j\frac{\eta}{k}\nabla' \bullet \mathbf{J}(\boldsymbol{r}')\nabla'\mathbf{G}_0(\boldsymbol{r},\boldsymbol{r}')\right] dS' \tag{11}$$

or in terms of the scattered field

$$\mathbf{E}^{\text{sca}}(r) = \int_S \left[j\frac{\eta}{k}\nabla' \bullet \mathbf{J}(\boldsymbol{r}')\nabla'\mathbf{G}_0(\boldsymbol{r},\boldsymbol{r}')\right] dS'. \tag{12}$$

The surface charge density is related to the surface current density through the equation of continuity (5), and

$$\nabla'\mathbf{G}_0(\boldsymbol{r},\boldsymbol{r}') = \hat{\mathbf{R}}\frac{(1+jk|\boldsymbol{r}-\boldsymbol{r}'|)}{4\pi|\boldsymbol{r}-\boldsymbol{r}'|^2}e^{-jk|\boldsymbol{r}-\boldsymbol{r}'|} \tag{13}$$

where $\hat{\mathbf{R}}$ is the unit vector along $(\boldsymbol{r}-\boldsymbol{r}\prime)$.

Utilizing (5) and (13), (12) can be written as

$$\begin{aligned}\mathbf{E}^{\text{sca}}(\boldsymbol{r}) &= \int_S \left[j\frac{1}{\omega\varepsilon}\nabla' \bullet \mathbf{J}(\boldsymbol{r}')\nabla'\mathbf{G}_0(\boldsymbol{r},\boldsymbol{r}')\right] dS' \\ &= \int_S \left[\frac{1}{\varepsilon}\left(-\frac{\nabla' \bullet \mathbf{J}(\boldsymbol{r}')}{j\omega}\right)\frac{(1+jk|\boldsymbol{r}-\boldsymbol{r}'|)}{4\pi|\boldsymbol{r}-\boldsymbol{r}'|^2}e^{-jk|r-r'|}\right]\hat{\mathbf{R}}dS' \\ &= \int_S \left[\frac{1}{\varepsilon}\rho(\boldsymbol{r}')\frac{(1+jk|\boldsymbol{r}-\boldsymbol{r}'|)}{4\pi|\boldsymbol{r}-\boldsymbol{r}'|^2}e^{-jk|r-r'|}\right]\hat{\mathbf{R}}dS'.\end{aligned} \tag{14}$$

At very low frequencies, i.e., $k \to 0$, (14) can be simplified to

$$\mathbf{E}^{\text{sca}}(r) = \int_S \left[\frac{\rho(\boldsymbol{r}')}{4\pi\varepsilon|\boldsymbol{r}-\boldsymbol{r}'|^2}\right]\hat{\mathbf{R}}dS' = -\mathbf{E}^{\text{inc}}(\boldsymbol{r}). \tag{15}$$

Equation (15) is the exact formula for the static electric field due to a distribution of charges. If the unknown charge density is represented by the divergence of RWG functions, as in (6),

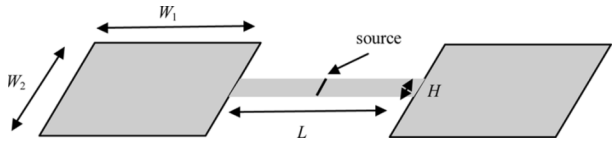

Fig. 1. Dipole antenna geometry.

and (15) is tested using RWG functions, the resulting moment method matrix equation is

$$\mathbf{C}_2 \cdot \mathbf{J} = \mathbf{F}. \tag{16}$$

The solution to (16) as the frequency approaches zero is the solution to the electrostatic problem. However, (16) cannot be solved directly because $\mathbf{C}_2$ is singular when closed loops exist. Note that for RWG basis functions, the unknown current density is defined on edges while the unknown charge density is defined on triangles. Since the number of edges is larger than the number of triangles, the static formulation is over-constrained and there are redundant rows in the $\mathbf{C}_2$ matrix. The LU recombination method can be used to solve this problem. Applying LU recombination to solve (16), (8) reduces to

$$\begin{bmatrix} \mathbf{D}_{2ii} & 0 \\ 0 & 0 \end{bmatrix} \begin{bmatrix} \mathbf{J}_i^r \\ \mathbf{J}_d^r \end{bmatrix} = \begin{bmatrix} \mathbf{F}_i^r \\ \mathbf{F}_d^r \end{bmatrix}. \tag{17}$$

This provides the solution for $\mathbf{J}_i^r$, and $\mathbf{J}_d^r$ can be set to zero. A solution for the original unknowns is then obtained using (9). This is not the correct solution for the total current distribution because the circulating part is neglected. However, this solution provides enough information to calculate the charge distribution using (6). Moreover, if the coefficient $j\omega$ is moved from the impedance matrix to the unknown, (16) becomes

$$[j\omega\mathbf{C}_2] \cdot \left[\frac{\mathbf{J}}{j\omega}\right] = \mathbf{F}. \tag{18}$$

This equation can be evaluated at zero frequency. The solution can then be employed to calculate the charge density using (6). Thus, with the help of LU recombination, the full-wave model can be applied directly to solve zero-frequency problems.

V. Numerical Results

Consider the dipole configuration shown in Fig. 1. The dipole is composed of two conducting patches and a strip connecting them. The dimensions of the patches are $W_1 \times W_2$ and the strip is $L \times H$. A voltage source is placed in the middle of the strip to raise the potential between the two patches to 1 V. The static charge density was calculated and the mutual capacitance obtained using a full-wave moment method code with LU recombination. The results are compared to those obtained using a static field solver, Q3D [15]. Table I lists the mutual capacitance calculated for dipoles with different dimensions. It also lists the difference between the full-wave and static field solver results.

It is worth noting that all metals are modeled as perfect electric conductors with zero thickness in the full-wave model. The source divides the structure into two conductors although there is no distance between them. In the static solver model, however, the metal has a nonzero thickness, and there is a small gap of 0.1 mm between the two conductors, so the charge distribution near the source is slightly different in the two models.

TABLE I
Capacitance of the Dipole Antenna

W_1 x W_2 (mm)	L x H (mm)	Full-wave (pF)	Static solver (pF)	Difference (%)	Source charge (pF)	% of total
50x50	100x10	1.667	1.953	14.6	0.1604	8.2
50x70	60x10	1.840	2.115	13.0	0.1610	7.6
50x50	100x2	1.377	1.472	6.4	0.0484	3.3
50x75	50x2	1.652	1.769	6.6	0.0489	2.8

Fig. 2. Parallel plate geometry.

TABLE II
Capacitance of Parallel Plates—10-mm Spacing
(Q3D Value: 42.0 pF)

Mesh type	Edge mesh density	# of triangles	Capacitance (pF)	Difference (%)
SC3_u	20 x 20	1656	37.8	10.0
SC3_b	20 x 20	1694	38.0	9.52
SC5_u	30 x 30	3692	38.9	7.38
SC5_b	30 x 30	3708	39.0	7.14
SC7_b	32 x 32	4194	39.3	6.43

Table I also shows the charge on the elements nearest the source in the full-wave model. This charge makes a relatively significant contribution to the total capacitance. Changing the size of the patches does not affect the percentage of this charge or the difference between the two models. This suggests that the source is the primary cause for the discrepancy between the two results. In this example, the difference is reduced if a narrower source strip is used.

The second example is a parallel plate capacitor as shown in Fig. 2. The size of the plates is 200 mm $\times$ 200 mm. The distance between them is 10 mm. The capacitor is charged to 1 V by a voltage source between the plates as shown.

Table II summarizes the capacitance calculated by the full-wave model, when different meshes were employed. The results are compared to the capacitance calculated using the static solver. For mesh type SC3_u, for example, the plate has 20 elements on one edge of the plate, and there are a total of 1656 triangular elements in the mesh. The calculated capacitance is 37.8 pF. The error is about 10% compared with the value obtained using the static solver.

TABLE III
CAPACITANCE OF PARALLEL PLATES— 40-mm SPACING
(Q3D VALUE: 14.536 pF)

Mesh type	Edge mesh density	# of triangles	Capacitance (pF)	Difference (%)
SC3_u	20 x 20	1666	13.38	7.72
SC3_b	20 x 20	1688	13.54	6.84
SC5_u	30 x 30	3748	13.643	6.14
SC9_b	60 x 60	2604	13.644	6.14

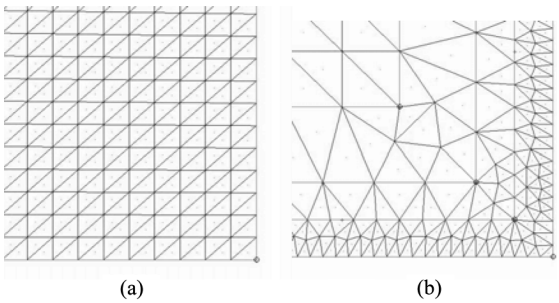

(a) (b)

Fig. 3. Parallel plate meshes: (a) SC5_u. (b) SC9_b.

The third example is also a parallel plate capacitor with 200 mm $\times$ 200 mm plates spaced 40 mm apart. A total of 5082 triangular patches were used by the static solver to obtain an accuracy of 0.1%. The results obtained using the full-wave model are listed in Table III, as well as the percent difference compared with the static solver results.

The results in Tables II and III demonstrate that the mesh geometry can be very important. A full-wave modeling code generally cannot afford to employ as many elements as a static field solver. Therefore, it is important to structure the mesh wisely.

Note that the results differ when using different types of meshes, even though the total number of elements is almost the same. In the meshing types, "u" indicates that the size of the elements is about the same, while "b" means the mesh is biased so that the elements near the edges are smaller. Fig. 3 compares the meshes SC5_u and SC9_b in Table III at one corner of the plate. The size of the element away from the edge in SC9_b is more than twice that in SC5_u, but the size of the element near the edge in SC9_b is about half of that in SC5_u. SC9_b yields a better result even though it employs a smaller number of elements.

VI. CONCLUSION

This paper presents a method to calculate static electric fields and charge distributions using full-wave boundary element software. An LU recombination approach is used to remove linearly dependent rows from the discretized scalar potential term of the EFIE. A considerable advantage of this method lies in the fact that neither special models, such as those used in the static and quasi-static methods, nor special basis functions, such as loop-tree basis functions, are necessary. The same models and methods used to perform a high-frequency analysis can be employed at arbitrarily low frequencies.

REFERENCES

[1] M. Burton and S. Kashyap, "A study of a recent moment-method algorithm that is accurate to very low frequencies," *Appl. Comput. Electromagn. Soc. J.*, vol. 10, no. 3, pp. 58–68, Nov. 1995.
[2] W. Wu, A. W. Glisson, and D. Kajfez, "A study of two numerical solution procedures for the electric field integral equation at low frequency," *Appl. Comput. Electromagn. Soc. J.*, vol. 10, no. 3, pp. 69–80, Nov. 1995.
[3] S. Kapur, D. Long, and J. Zhao, "Efficient full-wave simulation in layered, lossy media," in *Proc. IEEE Custom Integrated Circuits Conf.*, May 1998, pp. 211–214.
[4] J. Zhao and W. C. Chew, "Integral equation solution of Maxwell's equations from zero frequency to microwave frequencies," *IEEE Trans. Antennas Propagat.*, vol. 48, no. 10, pp. 1635–1645, Oct. 2000.
[5] W. Weeks, "Calculation of coefficients of capacitance of multiconductor transmission lines in the presence of a dielectric interface," *IEEE Trans. Microw. Theory Tech.*, vol. 18, no. 1, pp. 35–43, Jan. 1970.
[6] A. Ruehli and P. Brennan, "Efficient capacitance calculations for three-dimensional multiconductor systems," *IEEE Trans. Microw. Theory Tech.*, vol. MTT-21, no. 2, pp. 76–82, Feb. 1973.
[7] H. Nishiyama and M. Nakamura, "Form and capacitance of parallel-plate capacitors," *IEEE Trans. Comp., Packag., Manuf., Tech.*, vol. 17, no. 3, pp. 477–484, Sep. 1994.
[8] H. Ke and T. Hubing, "Using an LU recombination method to improve the performance of the boundary element method at very low frequencies," in *Proc. IEEE Int. Symp. Electromagn. Compat.*, Chicago, IL, Aug. 2005, pp. 442–445.
[9] H. Ke and T. Hubing, "A modified LU recombination technique for improving the performance of boundary element methods at low frequencies," *Appl. Comput. Electromagn. Soc. J.*, vol. 20, no. 3, pp. 178–185, Nov. 2005.
[10] Y. Ji, "Development and applications of a hybrid finite-element-method/method-of-moments (FEM/MOM) tool to model electromagnetic compatibility and signal integrity problems in printed circuit boards," Ph.D. dissertation, Dept. Electr. Comp. Eng., Univ. Missouri-Rolla, Rolla, MO, 2000.
[11] S. M. Rao, D. R. Wilton, and A. W. Glisson, "Electromagnetic scattering by surfaces of arbitrary shape," *IEEE Trans. Antennas Propagat.*, vol. 30, no. 3, pp. 409–418, May 1982.
[12] J. R. Mautz and R. F. Harrington, "An E-field solution for a conducting surface small or comparable to the wavelength," *IEEE Trans. Antennas Propagat.*, vol. 32, no. 4, pp. 330–339, Apr. 1984.
[13] A. Peterson, S. L. Ray, and R. Mittra, *Computational Methods for Electromagnetics*. Piscataway, NJ: IEEE Press, 1997, sec. Section 10.6, pp. 433–434.
[14] G. Gladwell and S. Coen, "A chebyshev approximation method for microstrip problems," *IEEE Trans. Microw. Theory Tech.*, vol. 23, no. 11, pp. 865–870, Nov. 1975.
[15] *Ansoft Corporation*, Q3D extractor 7.
[16] *Mentor Graphics Corporation*, HyperLynx 7.2.

Manuscript received April 25, 2006 (e-mail: hubing@clemson.edu).